AJNR

Chordomas of the skull base: MR features.

S P Meyers, W L Hirsch, Jr, H D Curtin, L Barnes, L N Sekhar and C Sen

AJNR Am J Neuroradiol 1992, 13 (6) 1627-1636
http://www.ajnr.org/content/13/6/1627

Chordomas of the Skull Base: MR Features

Steven P. Meyers,[1] William L. Hirsch, Jr.,[1] Hugh D.Curtin,[1,4] Leon Barnes,[2] Laligam N. Sekhar,[3] and Chandranath Sen[3]

PURPOSE: To characterize the MR features of skull base chordomas with regard to signal intensity, size, position, extension, and Gd-DTPA enhancement. **PATIENTS AND METHODS:** The MR imaging studies of 28 patients with surgically proven chordomas of the skull base were retrospectively reviewed. Twenty-two of these patients received intravenous administration of Gd-DTPA. **RESULTS:** On short TR/short TE images, chordomas generally had low to intermediate signal. On long TR/long TE images, chordomas generally had very high signal that was heterogeneous in 79%. After Gd-DTPA administration, all chordomas demonstrated some degree of contrast enhancement. In most cases, enhancement was demonstrated throughout most of each tumor in a heterogeneous pattern. Chordomas were associated with MR findings of displacement and encasement of vessels, and frequent extension into adjacent structures such as the cavernous sinus, sella, nasopharynx, and hypoglossal canal. **CONCLUSION:** The MR characterization of the position and extent of these neoplasms played an important role in determining the optimal surgical approaches for gross total tumor resection.

Index terms: Chordoma; Skull, base; Skull, magnetic resonance

AJNR 13:1627–1636, Nov/Dec 1992

Chordomas are uncommon slow-growing, destructive tumors (1–3). These neoplasms generally are locally invasive and rarely metastasize (2–8). Effective treatment of these often radiotherapy-insensitive lesions has been reported to depend upon surgical resection of as much tumor as possible (6, 9–13). Diagnostic imaging is important for preoperative assessment of tumor bulk and determining the anatomic relationship of tumor extension to adjacent neural, vascular, and bony structures (11).

We reviewed retrospectively the MR imaging studies of 28 patients with chordomas to characterize the unenhanced and gadopentetate dimeglumine (Gd-DTPA) enhanced features of these tumors with regard to: 1) signal intensity and 2) lesion size, position, and extension.

Materials and Methods

The MR imaging studies of 28 patients with skull base chordomas were reviewed retrospectively. The diagnosis of chordoma was established by histologic examination of the surgically removed specimens. Twenty-two of the chordomas were subclassified as conventional chordomas, and the other six as chondroid chordomas. With 26 patients, computed tomography (CT) scans were available for evaluation of bone erosion and tumor mineralization.

The patient group included 10 female and 18 male patients ranging in age from 3.5 to 74 years (mean age = 37 years, median age = 37 years). Sites of chordoma were: clivus (n=23) or petro-occipital junction (n=5). Fourteen patients with chordomas were imaged before initial surgical or radiation treatment. Two other patients had lesions biopsied and minimally resected 8 and 57 weeks prior to magnetic resonance (MR) imaging, which was performed in anticipation of definitive surgical resection (n = 1) or stereotactic radiosurgery (n = 1). Twelve patients had recurrent/residual chordomas imaged by MR 14 to 120 months after the initial surgery. Nine of these patients also had postoperative radiotherapy 14 to 48 months prior to the MR exam. Five of these

Received October 28, 1991; accepted and revision requested December 20; received February 12, 1992.

[1] Department of Radiology, University of Pittsburgh School of Medicine. Pittsburgh NMR Institute, Pittsburgh, PA 15213.

[2] Department of Pathology, University of Pittsburgh School of Medicine, Presbyterian-University Hospital, DeSoto at O'Hara Streets, Pittsburgh, PA 15213.

[3] Department of Neurosurgery, University of Pittsburgh School of Medicine, Presbyterian-University Hospital, DeSoto at O'Hara Streets, Pittsburgh, PA 15213.

[4] Address reprint requests to Hugh D. Curtin, MD, Department of Radiology, Presbyterian-University Hospital, DeSoto at O'Hara Streets, Pittsburgh, PA 15213.

AJNR 13:1627–1636, Nov/Dec 1992 0195-6108/92/1306-1627

patients received conventional photon radiotherapy with total dosages ranging from 5000 to 7000 cGy, one patient received 4000 cGy by stereotactic radiosurgery, and three patients received proton beam radiation of 60–70 cobalt gray equivalents. All of the patients with recurrent/residual chordomas had their lesions surgically resected after MR imaging.

MR imaging was performed at 1.5 T for 24 patients, at 0.5 T for three patients, and at 0.35 T for one patient. Multisection spin-echo pulse sequences were applied in all MR studies and included short TR (400–800 msec)/TE (20 msec) and long TR (2000–3200 msec)/first echo TE (25–30 msec), second echo TE (75–100 msec) sequences. MR images were obtained in the axial and sagittal planes. Most MR studies also included coronal plane images. MR images were 3–5 mm in thickness with an interimage gap of 1–2.5 mm. The acquisition matrix varied from 256 × 128 to 256 × 256.

MR imaging was performed immediately after the intravenous administration of Gd-DTPA (0.1 mmol/kg of body weight) for 22 patients (11 prior to histologic diagnosis/11 with recurrent/residual tumor). Postcontrast short TR (500–800 msec)/TE (20–30 msec) MR images were obtained in the sagittal and axial planes for all patients, and in the coronal plane for most patients.

For all images, the signal intensity of each tumor was assessed by two of the authors (S.P.M., W.L.H.) as hypo-, iso-, or hyperintense relative to muscle tissue, and gray and white matter in the field of view. Tumor signal was categorized as homogeneous, slightly (1+), or markedly (2+) heterogeneous for long TR/long TE images. The size, center-point, and extension of each tumor was determined. For postcontrast scans, the fraction of tumor volume showing enhancement was categorized as minimal (less than one-third), intermediate (one-third to two-thirds), or large (greater than two-thirds). The overall enhancement pattern of the tumors was graded as homogeneous, mildly (1+), or markedly (2+) heterogeneous. The degree to which parts or all of the tumors enhanced was qualitatively assessed as minimal (1+), intermediate (2+), or marked (3+).

The archived data of eight conventional chordomas and three chondroid chordomas imaged at 1.5 T were available for determination of T2 relaxation times using the software program of the MR imager (Signa, General Electric, Milwaukee, WI). Regions of interest within each tumor were drawn to eliminate the effects of volume averaging with adjacent structures. At least five measurements of the T2 relaxation times were made and averaged for each tumor. The mean and standard error of the T2 relaxation times for chondroid and conventional chordomas were calculated. The T1 relaxation times were not determined because none of the MR studies had the required minimum of two pulse sequences with different TRs and the same TE.

Noncontrast and contrast CT scans were performed with third-generation scanners. Tumors were evaluated for evidence of: 1) erosion and/or destruction of bone, and 2) intralesional mineralization.

Results

Size and Configuration of Chordomas

Chordomas imaged prior to display or surgery ranged in size from 1.0 × 1.0 × 1.5 cm to 6.0 × 6.0 × 6.5 cm with mean values of 3.5 × 3.2 × 4.1 cm in craniocaudal, anteroposterior, and transverse dimensions, respectively. Recurrent/residual chordomas ranged in size from 1.0 × 1.5 × 1.5 cm to 6.0 × 6.5 × 7.5 cm with mean values of 3.8 × 3.9 × 4.1 cm. Tumor borders were slightly multilobulated and well-defined except at sites of marrow invasion where the margins were often ill-defined.

Signal Characteristics of Chordomas

On short TR/TE images, chordomas generally had low to intermediate signal intensity (Figs. 1–5). Four lesions also had scattered small foci of very high signal on the short TR/TE images (Fig. 2). Histologic analysis of the resected specimens revealed small sites of hemorrhage and mucinous collections within these tumors that may account for the high signal characteristics. Two of these lesions were imaged prior to surgery and two after partial tumor resection. In 27 of 28 cases, chordomas had moderately high and very high signal on long TR/short TE and long TR/long TE images, respectively (Fig. 1–5). The one exception was a tumor that had zones of high, medium, and low signal on the long TR images (Fig. 6). Areas of low signal within this lesion were most pronounced on the long TR/long TE images at sites of magnetic susceptibility most likely from degraded blood products, ie, hemosiderin, which were demonstrated on histopathologic specimens. Tumor signal on the long TR/long TE images was homogeneous in 21% (Figs. 1, 3, and 5) mildly (1+) heterogeneous in 50% (Fig. 2), and markedly (2+) heterogeneous in 29% (Figs. 4 and 6). Comparisons of tumor signal relative to muscle, gray, and white matter are summarized in Table 1. No difference in signal characteristics was demonstrated between conventional and chondroid chordomas, nor between recurrent/residual lesions and those imaged prior to initial surgery.

Calculated T2 Relaxation Times

The T2 relaxation times of the conventional chordomas ranged from 85 to 133 msec with a

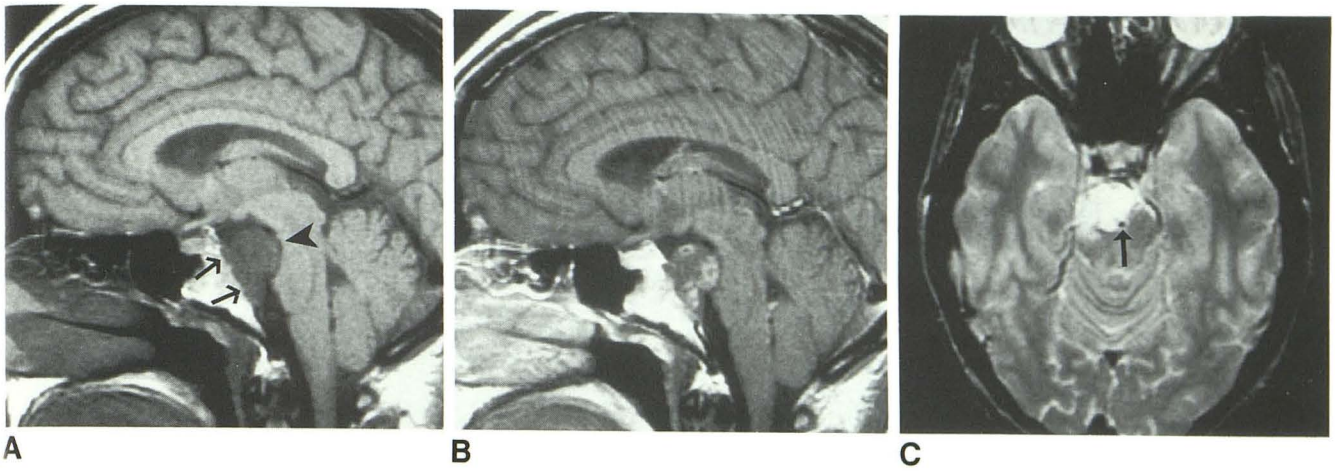

Fig. 1. A 29-year-old woman with a conventional chordoma imaged prior to initial surgery.

A, Precontrast short TR/TE 500/20 sagittal image (1.5 T) shows the lesion to involve the endocranial surface of the clivus (*arrows*). The tumor has isointense signal relative to muscle and is hypointense compared to gray and white matter. The lesion causes extrinsic compression of the pons (*arrowhead*) and extends slightly into the clivus marrow (*arrows*).

B, Postcontrast short TR/TE 550/20 sagittal image shows a minimal (1+) degree of enhancement within parts of the tumor in a markedly (2+) heterogeneous pattern.

C, Axial long TR/long TE 3000/80 image shows the mass to have homogeneous hyperintense signal relative to muscle, gray, and white matter. Posterior displacement of the basilar artery is noted (*arrow*).

mean value of 109 ± 7.0 (standard error of the mean). The T2 relaxation times of the chondroid chordomas ranged from 82 to 145 msec with a mean value of 119 ± 19 (standard error of the mean). Two of the three chondroid chordomas were imaged prior to initial surgical intervention or radiotherapy and had T2 values of 129 and 145 msec. According to the Mann-Whitney statistical test, no significant difference was demonstrated between the mean T2 values of conventional and chondroid chordomas at the $P < .05$ level.

Postcontrast Findings

Twenty-two patients had MR exams with images obtained before and immediately after intravenous administration of Gd-DTPA. All of the chordomas demonstrated contrast enhancement. The fraction of tumor demonstrating enhancement was large (greater than two-thirds) in 21 cases (Figs. 2, 3, and 4) and intermediate (one-third to two-thirds) in one case (Fig. 1). The degree to which tumors enhanced was qualitatively assessed as mild (1+) in six cases (Figs. 1 and 2), intermediate (2+) in seven cases, and marked (3+) in nine cases (Figs. 3 and 4). The overall enhancement pattern of chordomas was homogeneous in 19% (Fig. 3), mildly (1+) heterogeneous in 57% (Fig. 2), and markedly (2+) heterogeneous in 24% (Figs. 1 and 4).

Location and Extension of Chordomas

The center-points, and probable origination sites, of the 28 skull base chordomas were located within the basiphenoid-clivus (n = 6) (Fig. 2), within the basiocciput-clivus (n = 5) (Fig. 4), endocranial surface of sphenoid-clivus (n = 3), endocranial surface of occiput-clivus (n = 9) (Fig. 1), and at or near the petro-occipital junction (n = 5) (Figs. 3 and 4). MR showed extension of tumor into one (n = 15) or both (n = 3) cavernous sinuses (Fig. 2), sphenoid sinus (n = 6) (Fig. 2), ethmoid air cells (n = 5), sella (n = 12) (Figs. 2 and 3), suprasellar cistern (n = 7), orbits (n = 3), nasopharynx (n = 10) (Fig. 4), prestyloid (n = 4) and/or post-styloid (n = 3) parapharyngeal space, one (n = 8) or both (n = 2) hypoglossal canals (Fig. 4), jugular foramen (n = 4), and prevertebral space (n = 2) (Figs. 2 and 5). The tumor mass extended into the middle cranial fossa in nine patients (Figs. 2 and 5) and into the posterior fossa in 22 patients (Figs. 1, 2, and 4–6). None of the chordomas had extension into the anterior cranial fossa. MR demonstrated tumor displacement and partial encasement of one (n = 5) or both (n = 1) vertebral arteries, the basilar artery (n = 8) (Figs. 1, 2, and 4), or one (n = 6) (Fig. 5) or both (n = 2) internal carotid arteries. Tumor was shown to completely surround one (n = 1) or both (n = 1) vertebral arteries, the basilar artery (n = 1), and one (n = 8) or both (n = 1)

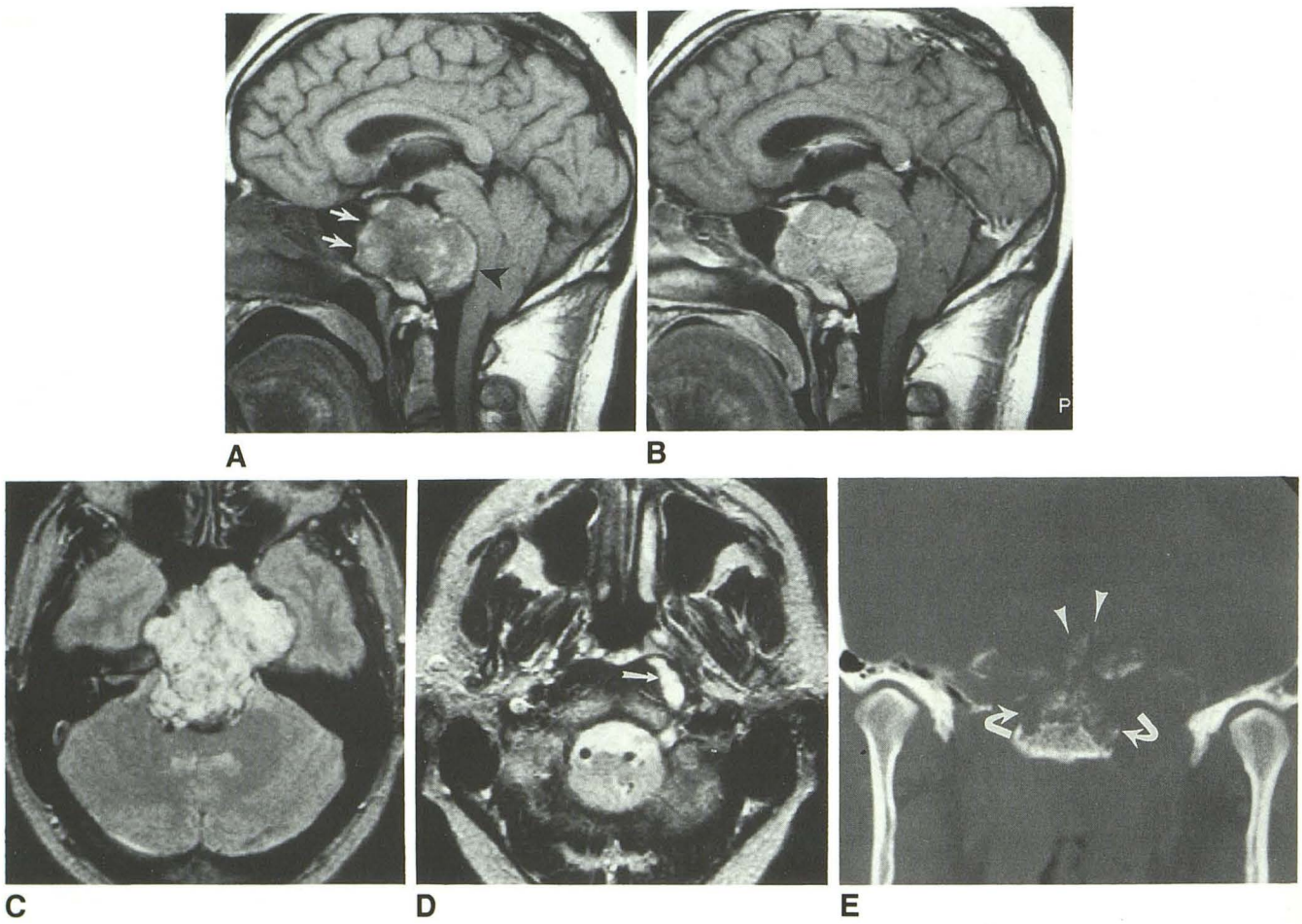

Fig. 2. A 36-year-old man with a conventional chordoma imaged prior to initial surgery.

A, Precontrast short TR/TE 500/20 sagittal image (1.5 T) shows the mass to be centered in the basisphenoid-clivus with extension anteriorly into the sphenoid sinus (*arrows*), and posteriorly resulting in marked mass effect on the pons and medulla (*arrowhead*). The tumor has heterogeneous signal with scattered small hyperintense foci representing sites of hemorrhage.

B, Postcontrast short TR/TE 500/20 sagittal image shows a minimal (1+) degree of enhancement throughout the tumor in a mildly (1+) heterogeneous pattern.

C, Long TR/long TE 2000/90 axial image shows the lesion to have mildly heterogeneous hyperintense signal relative to muscle, gray, and white matter.

D, Long TR/long TE 2000/90 axial image at the level of the foramen magnum shows tumor extension into the prevertebral space (*arrows*).

E, Coronal CT scan shows erosive bony changes (*curved arrows*) and scattered foci of mineralization or sequestered bone fragments within the tumor (*arrowheads*).

internal carotid arteries (Fig. 3). None of the arteries displaced or encased by chordomas had resultant luminal narrowing. Tumor borders were well defined by MR except at sites of marrow invasion where margins were irregular and indistinct. MR demonstrated tumor invasion of the marrow of the clivus (n = 28) (Figs. 1–4), petrous bone (n = 23) (Figs. 3 and 4), and one (n = 3) or both (n = 4) occipital condyles.

For 21 of the 28 chordomas, the center-points of lesions were located at or near midline within the clivus. Three other tumors were recurrent lesions that were eccentrically located within the clivus. The four remaining tumors, all imaged prior to surgery, had off-midline center-points located at or near the petro-occipital synchrondrosis. Of these four off-midline tumors, three were chondroid chordomas (Figs. 3 and 5) and one was a conventional chordoma.

Findings on CT

With 26 patients, CT scans were available for evaluation of intratumoral mineralization and bone erosion. All of the lesions had associated destructive and erosive bony changes demon-

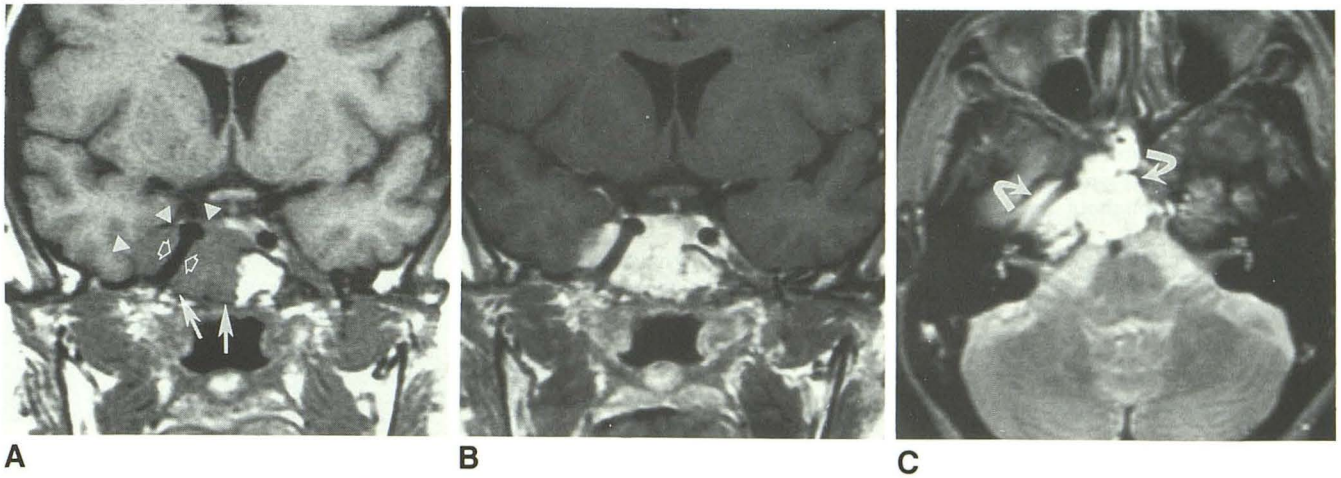

A B C

D

Fig. 3. A 53-year-old woman with a chondroid chordoma imaged prior to initial surgery.

A, Precontrast short TR/TE 500/20 coronal image (1.5 T) shows the tumor involving the clivus and petrous bone (*closed arrows*). The tumor extends superiorly into the sella, and laterally into the cavernous sinus (*arrowheads*) and carotid canal with encasement of the internal carotid artery (*open arrows*).

B, Postcontrast short TR/TE 500/20 coronal image shows predominantly homogeneous marked (3+) enhancement throughout the tumor.

C, Axial long TR/long TE 2600/80 image shows the tumor to have predominantly homogeneous hyperintense signal relative to muscle, gray, and white matter (*curved arrows*). Tumor encasement of the petrous portion of the internal carotid artery is also noted.

D, Coronal CT scan shows erosive and destructive bony changes in the right petro-occipital region by the tumor (*arrowheads*).

strated by CT (Figs. 2 and 3). Foci of mineralization or sequestered bone fragments were evident for seven of 26 lesions (Fig. 2). These foci were observed in one of six chondroid chordomas and six of 20 conventional chordomas. The pattern of mineralization consisted of a few scattered punctate densities. The MR exams did not show definite signal alterations at sites near where small calcific foci were seen on the CT scans.

Discussion

Chordomas are rare, slow-growing neoplasms that arise from rests of notochord cells (4–11, 14–21). The notochord is a primitive structure that serves as the embryonic precursor of parts of the skull base and spinal column (9, 15, 16, 18). The notochord arises during the fourth embryonic week and usually begins to regress by the seventh week as it is gradually replaced by mesodermal elements that eventually form the vertebrae and skull base (9, 16, 18). In autopsies of adults, remnants of notochordal tissue are occasionally found within bone most frequently from the cranial end of the dorsum sellae down to the caudal end of the coccyx, and rarely within the nasopharynx (6, 18).

Chordomas occur most frequently at the extreme ends of the spinal axis. In a large series of 155 chordomas, Heffelfinger et al (20) reported that 49% of the lesions were located in the sacrococcygeal region, 36% in the sphenooccipital, and 15% in the vertebral. Rare cases of chordoma arising within the nasopharynx and dura have also been reported (6, 16, 22). The large number of skull base chordomas in our series is reflective of the referral pattern to our institution which is an active skull base surgery center.

On gross pathologic examination, chordomas appear as lobulated, gelatinous, grayish tumors (3, 9, 20). Histologically, chordomas are composed of sheets of large vacuolated glycogen and/or mucin-containing cells (also called physaliferous cells) interspersed by fibrovascular

Fig. 4. A 19-year-old woman with a recurrent/residual conventional chordoma imaged 5 years after initial surgery and 2 years after radiotherapy (5500 cGy).

A, Short TR/TE 500/25 sagittal image (0.5 T) shows the mass to involve the clivus with extension posteriorly displacing the medulla (*arrowhead*), anteriorly into the nasopharynx (*closed arrow*), and inferiorly to involve the dens (*open arrow*).

B and C, Precontrast short TR/TE 480/25 axial image shows a large lobulated tumor (*arrows*) that on a postcontrast scan (*C*) shows a marked (3+) degree of enhancement throughout most of the tumor in a markedly (2+) heterogeneous pattern.

D, Long TR/long TE 2600/80 axial image shows the tumor to have heterogeneous predominantly hyperintense signal relative to muscle, gray, and white matter.

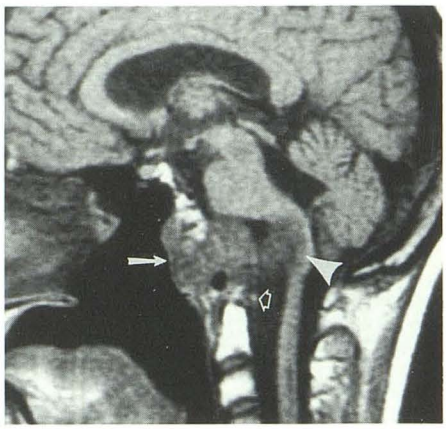

A

B C D

strands and cords of eosinopilic syncytial cells (15, 20). Chordomas also have varying amounts of extracellular mucinous matrix, entrapped bony trabeculae, small dystrophic calcifications, areas of necrosis, and recent and old hemorrhage (23, 24). Lesions containing chondroid elements have been subclassified into a group referred to as chondroid chordomas (15, 20, 25). The designation of chondroid chordomas as a subtype within the chordoma group is controversial (2, 23–26). Some recent immunohistochemical studies support the contention that chondroid chordomas may represent low-grade chondrosarcomas whereas others do not (2, 23–26). The fact that patients with chondroid chordomas have average survival times significantly longer than patients with conventional chordomas and similar to those with low-grade classical chondrosarcomas has also been used to support this hypothesis (3, 20). The issue, however, remains unsettled and continues to be debated (23–26).

Tumor signal on short TR/TE MR images was generally low to intermediate, predominantly hyper- or isointense relative to muscle, iso- or hypointense relative to gray matter, and hypointense compared to white matter. On MR images obtained with long TR/short TE and long TR/long TE sequences, both conventional and chondroid chordomas were generally high in signal intensity, which most likely reflects the high fluid content of vacuolated cellular components. Previous reports similarly have characterized chordomas as having moderately or extremely high signal intensity on long TR/long TE images (1, 7, 8). These previous studies, however, did not include comparisons of tumor signal relative to other tissues within the field of view (1, 7, 8). In addition, many of these studies included MR exams performed predominantly at low or intermediate field strengths (1, 7, 8).

Signal heterogeneity of chordomas on long TR/TE images was observed in 79% of the

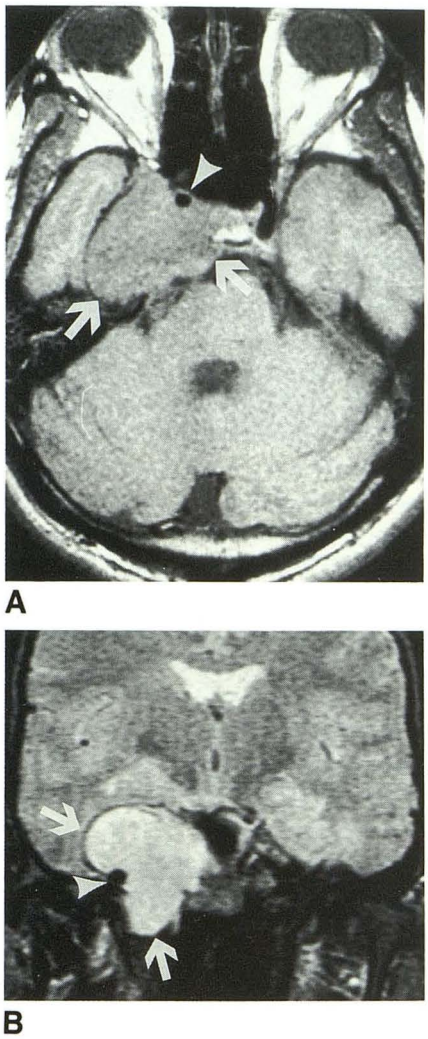

Fig. 5. A 21-year-old man with a chondroid chordoma imaged prior to initial surgery.

A, Short TR/TE 600/20 axial image (1.5 T) shows the mass involving the clivus and petrous bone (*arrows*). The tumor extends into the cavernous sinus and partially encases the internal carotid artery (*arrowhead*).

B, Long TR/long TE 2500/75 coronal image shows an off-midline mass that has high signal. The tumor partially encases the petrous carotid artery (*arrowhead*) and extends into the middle fossa and prevertebral space (*arrows*).

lesions. Chordomas were usually resected or suctioned in small pieces because of the limited surgical exposure and soft gelatinous texture of these tumors. As a result, direct histopathologic-imaging correlation could not be performed. Review of several resected specimens showed varying amounts of fibrovascular tissue, necrotic zones, pools of mucinous matrix, recent and remote hemorrhage, and entrapped bony trabeculae. The variability of these components may explain the observed signal heterogeneity, but we were unable to do a definite correlation.

By CT, scattered small foci of calcification/mineralization were observed in six of 20 conventional chordomas and one of six chondroid chordomas. As described previously (1, 19), it is often difficult or impossible to distinguish sequestered bone fragments from tumor calcification in chordomas using CT. The MR exams were not effective in demonstrating definitive signal alterations at the sites of small calcific foci, within the tumors. The lack of visualization of these foci by MR is probably related to their very small size and number as well as volume averaging effects and difference in the planes of imaging.

No difference in MR signal characteristics was demonstrated between recurrent/residual tumors and those imaged prior to surgery or radiotherapy. Sze et al (7) previously reported that, on long TR/long TE images, chondroid chordomas had moderately high signal that was lower relative to conventional chordomas. These workers also reported that some, but not all, chondroid chordomas had lower T1 and T2 values compared to conventional chordomas (7). In our series, no overall qualitative difference in MR signal characteristics was observed between conventional and chondroid chordomas. In addition, the chondroid chordomas had a slightly higher mean T2 value than conventional chordomas, although the difference was not significant at the $P < .05$ level. These results suggest that it may not be possible to use the MR signal characteristics of chordomas for distinguishing between the chondroid and conventional types as previously suggested by Sze et al (7).

To our knowledge, Gd-DTPA-enhancement characteristics of chordomas have not been previously reported for any series. All of the chordomas demonstrated Gd-DTPA contrast enhancement of varying degrees. In most cases, enhancement was demonstrated throughout most of each tumor in a heterogeneous pattern. Because chordomas generally enhanced with Gd-DTPA to a greater degree than brain parenchyma, postcontrast exams often helped in defining tumor margins relative to adjacent neural tissue. Tumor margins adjacent to fatty tissues such as marrow, however, were usually less well-defined on postcontrast scans relative to the unenhanced scans. All postcontrast images in our series were acquired immediately after

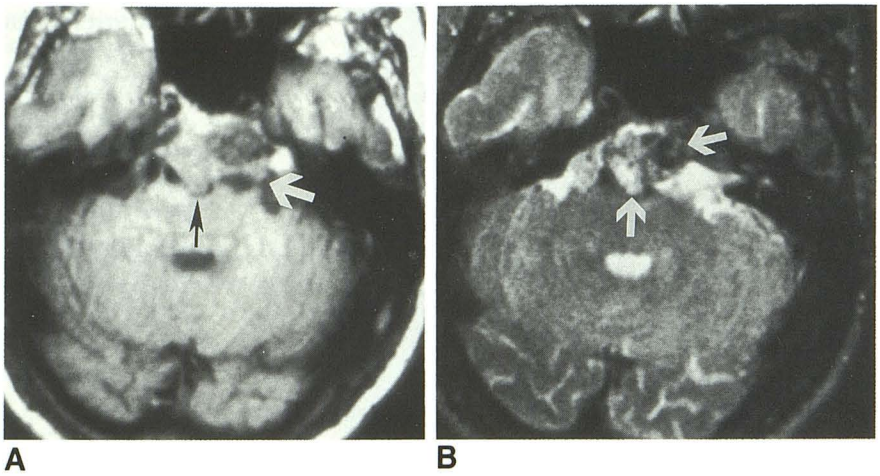

Fig. 6. A 74-year-old man with a conventional chordoma imaged prior to surgery.

A, Short TR/TE 550/30 axial image (1.5 T) shows the tumor involving the endocranial surface of the clivus (*arrows*). The tumor has mixed signal with areas of intermediate and low signal.

B, Long TR/long TE 2500/100 axial image shows tumor signal heterogeneity with areas of low, intermediate, and high signal (*arrows*).

TABLE 1: Signal intensity of chordomas

	Signal Intensity in Relation to Muscle (%)[a]				Signal Intensity in Relation to Gray Matter (%)				Signal Intensity in Relation to White Matter (%)			
	hyper	iso	hypo	mixed	hyper	iso	hypo	mixed	hyper	iso	hypo	mixed
On T1W images	61	25	3	11	3	36	43	18		7	79	14
On PD images	96			4	75	18		7	96			4
On T2W images	96			4	92	4		4	96			4

Note.—T1W = short TR/short TE spinecho; PD = long TR/short TE spinecho; T2W = long TR/long TE spinecho; hyper = hyperintense; iso = isointense; hypo = hypointense.

[a] % = percent of lesions with these predominant signal characteristics.

Gd-DTPA administration. Therefore, it is unknown what effects delaying the time to imaging after contrast administration might have on the degree, extent, and pattern of tumor enhancement. The MR enhancement findings of chordomas with Gd-DTPA are analogous to those reported with CT using iodinated contrast (20).

Chordomas have been considered to be generally midline lesions as a result of the position of most notochordal tissue remnants (8, 14, 16, 18). Rarely, cranial chordomas have been reported to arise in off-midline locations where residual branches of notochordal tissue are thought to occur within the skull base and nasopharynx (6, 14, 16). Off-midline chordomas have been described arising within the petrous apex and Meckel's cave (14, 16). Of the chordomas in our series, 21 had midline center-points within the clivus. Three other lesions were recurrent chordomas eccentrically located within the clivus. The slightly off-midline locations of these chordomas might be related to recurrence at sites of unresected tumor rather than to actual origination sites. The remaining four lesions were evaluated on preoperative MR and included three chondroid chordomas and one conventional chordoma that had off-midline center-points located at the petro-occipital junction. It is noteworthy that these three chondroid chordomas involved the petro-occipital synchondrosis, a site where cranial chondrosarcomas predominate (27). Of the 14 tumors imaged prior to surgery or radiotherapy, nine (90%) of ten conventional chordomas were midline in location, whereas two (50%) of four chondroid chordomas had midline center-points. These two midline chondroid chordomas were located near the spheno-occipital synchondrosis, another site where chondrosarcomas occur (27). Although the number of chondroid chordomas imaged prior to surgery is small, our results suggest that when chordomas of the skull base have off-midline center-points they are more likely to be of the chondroid type rather than conventional.

Chordomas are locally invasive tumors as evidenced by destructive and erosive bony changes on CT scans, and MR findings of marrow invasion and extension into adjacent structures. Skull base chordomas often extended into the posterior cranial fossa and, to a lesser extent, the middle fossa. The MR exams showed frequent tumor invasion into the cavernous

sinus, sella, nasopharynx, and hypoglossal canal. MR was extremely useful in showing the anatomic relationship of tumor to major intracranial vessels. Tumor displacement or partial encasement of one or more intracranial arteries was demonstrated by MR in 79% of the skull base chordomas. Complete tumor encasement of at least one artery was observed in 43% of the chordomas. It is interesting to note that none of the arteries encased by chordomas had resultant luminal narrowing. The lack of arterial narrowing by chordomas may correlate with the neurological observation that these tumors are generally soft and easily dissected off adjacent vessels (11). MR has been reported to be superior to angiography in detecting vascular encasement by tumor (28). Angiographic documentation of encasement relies on indirect findings of extrinsic luminal narrowing that may not be present as in the chordomas in this series. Defining the anatomic relationship of tumor with the internal carotid artery is important for preoperative planning because of the potential for permanent occlusion of this vessel from surgery (11, 29). To test whether patients are at risk for neurologic injury due to permanent vessel occlusion, intraluminal balloon test occlusion of the internal carotid artery can be used in conjunction with clinical evaluation and imaging of cerebral blood flow using stable xenon-enhanced CT scans (11, 29). Those patients at risk for neurologic injury from compromised cerebral blood flow can have placement of arterial bypass grafts to prevent this potential complication (11, 29).

Surgical resection of as much tumor as possible has been reported to be the most effective treatment of chordomas (11). Recent advances in the field of skull base surgery has made gross total tumor removal possible (11, 30, 31). MR imaging, with its multiplanar imaging capability and high contrast resolution, has played an important role in the preoperative evaluation of the location and extent of these neoplasms (11). Such information is critical for determining the optimal surgical approach(es) in attempting total tumor resection (11, 30, 31). For clival chordomas that extend into the ethmoid and sphenoid sinuses, the basal subfrontal approach has been an effective method (11, 30, 31). Tumors that extend lateral to the petrous internal carotid arteries, however, cannot be reached by this technique (11, 30, 31). In these situations, the subtemporal and preauricular infratemporal approach to the middle and posterior cranial base can be used (11, 30). When chordomas are very large and involve both the sphenoid and ethmoid sinuses as well as the petrous bones, the subfrontal transbasal and infratemporal approaches are combined (11, 30). Both of these surgical approaches are primarily extradural (11). When tumors involve the superior sphenoid-clivus and extend into the suprasellar cistern and/or cavernous sinus, an intradural approach is used to supplement the main extradural part of the surgical procedure (11). In most cases, gross total tumor resection can be achieved with low morbidity (11). When a small residual tumor is identified by MR, precision high-dose radiotherapy has been shown to be beneficial in some cases (13, 32, 33).

The differential diagnosis of skull base chordomas includes chondrosarcomas, meningioma, metastases, pituitary adenoma, epidermoid, chondroma, plasmacytoma, and paraganglioma. A midline lesion involving the clivus that has very high signal on long TR/long TE images, shows heterogeneous enhancement with Gd-DTPA, and is associated with erosive bony changes strongly favors the diagnosis of chordoma. Definitive diagnosis based solely on MR characteristics, however, may not be possible. The important clinical role of MR is to define tumor size and location, as well as determining the anatomic relationship of tumor extension to adjacent normal vascular, neural, and bony structures.

Acknowledgments

The authors thank Dr Steven Tresser, Dr Nancy Tresser, Dr Douglas Kondziolka, and Dr L Dade Lunsford for contributing case materials, and Mary Bialik and Kathryn Frazier for assistance in the preparation of this manuscript.

References

1. Larson TC III, Houser OW, Laws ER Jr. Imaging of cranial chordomas. *Mayo Clin Proc* 1987;62:886–893
2. Russell DS, Rubinstein LJ. Chondrosarcomas and chordomas. In: *Pathology of tumours of the nervous system*. Baltimore: Williams & Wilkins, 1989:819–821
3. Rich TA, Schiller A, Suit HD, Mankin HJ. Clinical and pathologic review of 48 cases of chordoma. *Cancer* 1985;56:182–187
4. Krol G, Sze G, Arbit E, Marcove R, Sundaresan N. Intradural metastases of chordoma. *AJNR* 1989;10:193–195
5. de Bruïne FT, Kroon HM. Spinal chordoma: radiologic features in 14 cases. *AJR* 1986;150:861–863
6. Singh W, Kaur A. Nasopharyngeal chordoma presenting with metastases: case report and review of literature. *J Laryngol Otol* 1987;101:1198–1202

7. Sze G, Uichanco LS III, Brant-Zawadzki MN, et al. Chordomas: MR imaging. *Radiology* 1988;166:187–191
8. Oot RF, Melville GE, New PFJ, et al. The role of MR and CT in evaluating clival chordomas and chondrosarcomas. *AJR* 1988; 151:567–575
9. Yuh WTC, Lozano RL, Flickinger FW, Sato Y, Kao SSC, Menezes AH. Lumbar epidural chordoma: MR findings. *J Comput Assist Tomogr* 1989;13:508–510
10. Raffel C, Wright DC, Gutin PH, Wilson CB. Cranial chordomas: clinical presentation and results of operative and radiation therapy in twenty-six patients. *Neurosurgery* 1985;17:703–710
11. Sen CN, Sekhar LN, Schramm VL, Janecka IP. Chordoma and chondrosarcoma of the cranial base: an 8-year experience. *Neurosurgery* 1989;25:931–941
12. Cummings BJ, Hodson DI, Bush RS. Chordoma: the results of megavoltage radiation therapy. *Int J Radiation Oncol Biol Phys* 1983;9:633–642
13. Suit HD, Goitein M, Munzenrider J, et al. Definitive radiation therapy for chordoma and chondosarcoma of base of skull and cevical spine. *J Neurosurg* 1982;56:377–385
14. Brown RV, Sage MR, Brophy BP. CT and MR findings in patients with chordomas of the petrous apex. *AJNR* 1990;11:121–124
15. Matsumoto J, Towbin RB, Ball WS Jr. Cranial chordomas in infancy and childhood: a report of two cases and review of the literature. *Pediatr Radiol* 1989;20:28–32
16. Yuh WTC, Flickinger FW, Barloon TJ, Montgomery WJ. MR imaging of unusual chordomas. *J Comput Assist Tomogr* 1988: 12:30–35
17. Rosenthal DI, Scott JA, Mankin HJ, Wismer GL, Brady TJ. Sacrococcygeal chordoma: magnetic resonance imaging and computed tomography. *AJR* 1985;145:143–147
18. Bonneville JF, Belloir A, Mawazini H, et al. Calcified remnants of the notochord in the roof of the nasopharynx. *Radiology* 1980; 137:373–377
19. Meyer JE, Oot RF, Lindfors KK. CT appearance of clival chordomas. *J Comput Assist Tomogr* 1986;10:34–38
20. Heffelfinger MJ, Dahlin DC, MacCarty CS, Beabout JW. Chordomas and cartilaginous tumors at the skull base. *Cancer* 1973;32: 410–420
21. Meyer JE, Lepke RA, Lindfors KK, et al. Chordomas: their CT appearance in the cervical, thoracic and lumbar spine. *Radiology* 1984;153:693–696
22. Mapstone TB, Kaufman B, Ratcheson RA. Intradural chordomas without bone involvement: nuclear magnetic resonance (NMR) appearance. Case report. *J Neurosurg* 1983;59:535–537
23. Barnes L. Pathology of selected tumors of the base of the skull. *Skull Base Surgery* 1991;1:207–216
24. Barnes L. Chordoma. In: *Surgical pathology of the head and neck*. New York: Marcel Dekker, 1985:967–971
25. Huvos AG. Chordoma. In: *Bone tumors: diagnosis, treatment, and prognosis*. 2nd ed. Philadelphia: Saunders, 1991:599–624
26. Brooks JJ, LiVolsi VA, Trojanowski JQ. Does chondroid chordoma exist? *Acta Neuropathol (Berl)* 1987;72:229–235
27. Meyers SP, Hirsch WL, Curtin HD, et al. Chondrosarcomas of the skull base: MR imaging features. *Radiology* 1992;184:103–108
28. Young SC, Grossman RI, Goldberg HI, et al. MR of vascular encasement in parasellar masses: comparison with angiography and CT. *AJNR* 1988;9:35–38
29. Erba SM, Horton JA, Latchaw RE, et al. Balloon test occlusion of the internal carotid artery with Xenon/CT cerebral blood flow imaging. *AJNR* 1988;9:533–538
30. Sekhar LN, Schram VL, Jones NF. A subtemporal and preauricular infratemporal fossa approach to large lateral and posterior cranial base neoplasms. *J Neurosurg* 1987;67:488–499
31. Sekhar LN, Janecka IP, Jones NF. Subtemporal-infratemporal and basal subfrontal approach to extensive cranial base tumors. *Acta Neurochir* 1988;92:83–92
32. Austin-Seymour M, Munzenrider J, Goitein M, et al. Fractionated proton radiation therapy of chordoma and low-grade chondrosarcoma of the bias of the skull. *J Neurosurg* 1989;70:13–17
33. Kondziolka D, Lunsford LD, Flickinger JC. The role of radiosurgery in the management of chordoma and chondrosarcoma of the cranial base. *Neurosurgery* 1991;29:38–46